

Electrostatic Field and Partial Fermi Level Pinning at the Pentacene–SiO₂ Interface

Liwei Chen,^{†,§} R. Ludeke,[‡] Xiaodong Cui,[†] Alejandro G. Schrott,[‡] Cherie R. Kagan,[‡] and Louis E. Brus^{*,†}

Department of Chemistry, Columbia University, New York, New York 10027, and IBM T. J. Watson Research Center, Yorktown Heights, New York 10598

Received: August 11, 2004; In Final Form: October 27, 2004

Monolayer islands of pentacene deposited on silicon substrates with thermally grown oxides were studied by electric force microscopy (EFM) and scanning Kelvin probe microscopy (SKPM) in ultrahigh vacuum (UHV) after prior 10 min exposure to atmospheric ambient. On 25-nm-thick oxides, the pentacene islands are 0.5 V higher in electrostatic potential than the silicon dioxide background because of intrinsic contact potential differences. On 2-nm-thin oxides, tunneling across the oxides allows Fermi level equilibration with pentacene associated states. The surface potential difference depends on the doping of the underlying Si substrates. The Fermi level movement at the pentacene SiO₂ interface was restricted and estimated to lie between 0.3 and 0.6 eV above the pentacene valence band maximum. It is proposed that hole traps in the pentacene or at the pentacene–oxide interface are responsible for the observations.

Introduction

Organic semiconductors, most notably pentacene, have attracted attention as channel materials in thin film transistors (TFTs) since these devices have field-effect mobilities of ~ 1 cm²/V-sec and current modulation of $\sim 10^7$ – 10^8 .^{1–4} In TFTs, current modulation is restricted to the accumulation layer, believed to be within a countable number of molecular monolayers at the interface with the gate dielectric. Thus, charge carrier transport in the accumulation layer of TFTs may be very different from that probed by time-of-flight measurements in bulk crystals.^{5–8} The interface between the organic semiconductor and the gate dielectric plays a crucial role in the thin accumulation layer.

Relatively few studies have attempted to characterize the interface or impurity states in pentacene TFTs. In one study, a distributed trap model with a steep exponential tail of donors and a shallower exponential tail of acceptors inside the band gap was proposed to describe the experimental current–voltage characteristics.⁹ Capacitance–voltage and deep-level transient spectroscopy measurements were also performed on pentacene TFTs.¹⁰ Hole traps at 0.24, 0.31, and 1.08 eV above the valence band maximum and electron traps at 0.69 eV below the conduction band minimum were observed.

To further understand the device physics, it is necessary to study the interface directly. Here, we use electric force microscopy (EFM) in ultrahigh vacuum (UHV) to locally probe the electrostatic properties of the first pentacene layer at the interface with a gate oxide. As a variation of scanning probe microscopy, the EFM technique inherits the capability of local imaging on insulating samples. It has been previously used to probe localized charge traps and dangling bond states in silicon oxide with very high sensitivity.^{11,12} In addition to probing E-fields on surfaces, it measures local surface potential differ-

ences by adjusting a DC bias voltage between the tip and the sample to zero out the field. This closed-loop technique is also referred to as scanning Kelvin probe microscopy (SKPM) and has been used to map electrostatic potential in PN junctions¹³ and organic TFTs.¹⁴ Furthermore, EFM and SKPM provide a measure of the Fermi level of pentacene thin films. When a thin oxide layer is used on the substrate, electron tunneling through the barrier happens fast enough such that an electric equilibrium between the sample and the Si substrate is established within the experimental time scale.¹⁵ With the establishment of Fermi level alignment and the measurement of vacuum level shift, the position of Fermi level within the organic semiconductor band gap can be extracted.

Experimental Section

Pentacene thin films on SiO₂ were prepared by thermal deposition in high vacuum. Degenerately doped silicon substrates with thermally grown oxide layers (IBM Research, Yorktown Heights, NY) were first sonicated twice in chloroform for 10 min and then cleaned in UV-ozone for 30 min. The substrates were quickly loaded into a vacuum chamber (5×10^{-9} Torr) and heated at 300 °C for 2 h. The substrates were then held at 30 °C and pentacene was evaporated in the same chamber at a rate of 0.1 monolayers per min for ~ 2 min to deposit submonolayer pentacene islands.

The as-evaporated sample was transported in atmospheric ambient from the evaporation chamber to the EFM chamber in about 10 min. The EFM experiments were conducted over a period of days in a JEOL A4500 UHV ($1 \sim 2 \times 10^{-10}$ Torr) AFM using tungsten carbide coated conducting AFM tips (MikroMasch, Portland, OR). In the EFM experiments, the AFM operates in the intermittent contact mode with the tip touching the sample at the bottom of its 4-nm oscillation cycles. Unlike ambient EFM in which the electric force gradient is obtained in a separate scan line from the topography,¹⁶ the JEOL vacuum EFM simultaneously obtains the topography and electric force gradient in one scan line with a bias voltage applied throughout the scan. The total force on an EFM tip is the combination of

* Corresponding author. E-mail: leb26@columbia.edu.

[†] Columbia University.

[§] Current address: Department of Chemistry and Biochemistry, Ohio University, Athens, OH 45701.

[‡] IBM T. J. Watson Research Center.

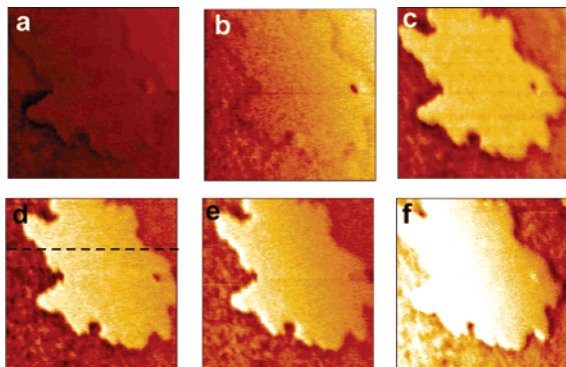


Figure 1. EFM images of pentacene islands on 25-nm SiO₂ at various bias voltage (a) -0.8 V (b) -0.6 V (c) -0.5 V (d) 0 (e) 0.2 V (f) 0.4 V. The scan size for all images is 800 nm.

the capacitive force, the Coulomb interaction, the van der Waals force, and the hard-sphere repulsion:

$$F_{\text{EFM}} = \frac{1}{2} \frac{dC}{dz} (V_b + \varphi)^2 - E_z C (V_b + \varphi) + F_{\text{VDW}} + F_{\text{hs}}$$

where F_{VDW} is the van der Waals force, F_{hs} is the hard-sphere repulsion when the tip and the sample are in very close contact, V_b is the bias voltage applied to the sample, φ is the surface potential difference between the tip and substrate, and C is the tip-sample capacitance including Si substrate and SiO₂ dielectric only. E_z is the static field due to charges or multipoles of the sample excluding the field of charges accumulated on capacitor plates, namely, the tip and the substrate under bias voltages. E_z has two components, E_z^{S} due to static charges and multipoles, and E_z^{ind} , due to polarization induced in the sample by the bias field. The sign of vectors such as force and field is assigned to be positive when pointing away from surface.

The EFM detects the shift in tip resonance frequency $\Delta\nu$ due to force gradients. When the van der Waals force and the hard-sphere repulsion dominate the overall interaction, the sample surface topography is followed by the tip via a feedback loop that controls the Z-piezo displacement to hold the tip resonance frequency at a constant, typically 10–20 Hz higher than the free resonance (this feedback is different from the usual amplitude feedback in ambient AFM). The electric force gradient is measured by adding a small low-frequency modulation to V_b and demodulating the frequency shift signal with a lock-in amplifier. We chose the phase of the lock-in amplifier to follow the convention that darker portions in the E-force gradient images represent regions of relative potentials that are more negative than those in the lighter areas, or equivalently, the latter are more positive.¹¹

SKPM measurements are carried out in true noncontact mode, in which a negative frequency shift set point is used. The tip oscillates within the attractive force regime.

Results

A. 25-nm-Thick Oxide. Figure 1 shows EFM images of a pentacene sample deposited on n-type Si with a 25-nm silicon dioxide taken with a bias voltage ranging from -0.8 to $+0.4$ V. In these images, the contrast between the bare oxide surface and the pentacene island is strongly dependent on the applied bias voltage. At zero bias (Figure 1d), the pentacene island appears brighter than the SiO₂ background. This indicates the scanning probe feels an electric field with the direction of positive charges or electric dipoles with the positive end pointing out of the surface or, equivalently, the surface potential on the

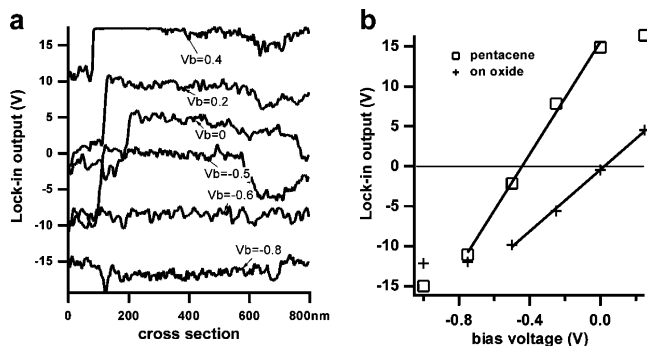


Figure 2. (a) Electric force profile across the pentacene island at the cross section labeled in Figure 1d. The offset in the pentacene island position is due to the scanner drift among the scans. (b) Electric force gradient averaged over a long time on pentacene and on silicon dioxide at various bias voltages.

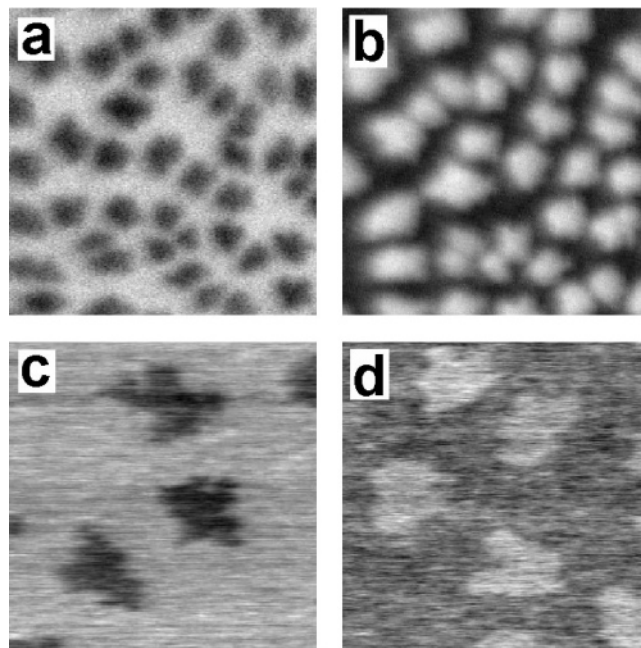


Figure 3. Kelvin probe images of the pentacene islands: (a) and (c) on n-type Si with 2-nm SiO₂; (b) and (d) on p-type Si with 2-nm SiO₂. Scan size: (a) and (b) $3 \mu\text{m}$; (c) and (d) $1.5 \mu\text{m}$.

pentacene island is higher than that on the SiO₂ background. The bias dependent contrast is illustrated in electric force line profiles shown in Figure 2a. At zero bias, a contrast of ~ 7 V in lock-in output, which serves as an arbitrary unit for electric field gradients in this discussion, is observed. When negative bias voltages are applied to the sample, the difference in electric force gradient becomes smaller. At -0.6 V bias, little contrast is seen between the pentacene island and the oxide surface and at an even more negative voltage of -0.8 V, the contrast in electric force gradient is reversed. On the other hand, the observed contrast in electric force gradient is enhanced at positive applied bias. The average force gradient as a function of bias is more accurately measured by reading the lock-in output and averaging over longer time while the tip resides either on the pentacene or on the oxide. The results are plotted in Figure 2b.

B. 2-nm-Thin Oxide. The interface properties were drastically different for thin 2-nm oxides. As shown in SKPM images in Figure 3, the surface potential of pentacene becomes lower than the oxide on an n-type substrate (Sb-doped, 0.008 – $0.03 \Omega\text{-cm}$) with a 2-nm oxide, as opposed to being higher than the oxide for a 25-nm-thick oxide layer on the same n-type substrate.

TABLE 1: Relative Vacuum Level with Respect to the Scanning Probe in UHV and in 0.1 Pa O₂

in UHV	SiO ₂	pentacene
p-Si	-0.37 V	-0.19 V
n-Si	0.09 V	0
in O ₂	SiO ₂	pentacene
p-Si	-0.77 V	-0.61 V
n-Si	-0.3 V	-0.38 V

The contrast is reversed on a p-type substrate (B-doped, 0.005–0.01 Ω-cm) with a 2-nm oxide. Statistics on multiple images shows that the pentacene surface potential is 0.09 V lower than SiO₂ on the n-type substrate while it was 0.18 V higher than SiO₂ on the p-type substrate. The relative positions of the vacuum level of pentacene and SiO₂ on p- and n-type Si substrates with respect to the vacuum level of the scanning probe were obtained from these images and are summarized in Table 1.

After the SKPM imaging in UHV over 2 days, we filled the chamber with about 0.1 Pa (0.75 mTorr) of oxygen and the pentacene samples were imaged again with SKPM for about 2 h. The resulting images have no apparent changes from the images in UHV. A short exposure to oxygen has no measurable effect for our samples which have been previously exposed to ambient, other than an overall shift in the vacuum level of ~0.4 eV (Table 1).

Discussion

Interface Dipole on Thick Oxide. The observed contrast in Figure 1 shows a significant difference between the electrostatic fields on the pentacene island and on the SiO₂ substrate. The contrast does not appear to arise from bias-dependent charging of the pentacene island. This notion is based on the following observation. Work function, ionization potentials, and electron affinity data for pentacene and W₂C (the tip material)^{17,18} suggest that the Fermi level of the tip lies well within the pentacene band gap and charging the pentacene should not be possible for moderate biases as there are no available states that would enable tunneling of charge between tip and sample. While we cannot rule out entirely the presence of trapped positive charges, the uniformity of the signal across the island suggests that such fixed charge cannot explain the observed contrast. We propose here that the contrast is due to an interfacial dipole in the pentacene. The measurement does not distinguish whether the dipole extends into the pentacene or appears locally between the oxide and the pentacene monolayer. However, we have no evidence for a dipole localized at the interface. Instead, we argue for a dipole across the pentacene layer that arises from contact potential differences between the SiO₂ and the pentacene layer and the polarizability of the pentacene. The shift of charge upon contact between two dielectrics depends on their respective charge neutrality levels (CNL), which for SiO₂ has been calculated to be 4.8 eV below the vacuum level, or nearly midway between the valence and conduction bands.¹⁹ Assuming that the CNL of pentacene lies similarly near midgap or 4 eV below the vacuum level, the electron density would consequently shift toward the SiO₂ interface leaving the vacuum end of the pentacene molecules more positive. The resulting dipole exhibits the correct polarity that can be inferred from the experiment, that is, an enhanced (brighter) contrast than that observed on the SiO₂. Applying a positive bias enhances the charge separation in the pentacene presumably because of its greater polarizability. A negative bias diminishes and even reverses the

dipole, with some evidence of contrast reversal seen in Figure 1a for the largest (−0.8 V) bias. The electric field gradient is changed as well on the SiO₂, as can be verified by the line profiles in Figure 2a.

Spatial variation in the EFM images over SiO₂ exceeds instrument noise and reflects real fluctuations of the surface field gradient. The local variations are very similar to previous studies on SiO₂ that were assigned to individual charge centers and trapped states.^{11,12} The fluctuations on pentacene islands are consistently smaller than those on the SiO₂ background. This suggests that the interface dipole is evenly distributed over the entire island and the inhomogeneous field that originates from charge centers in SiO₂ becomes smoother on pentacene islands. The latter could be due to two reasons: (1) the EFM tip is 1.8 nm further away from the charge centers and thus experiences a more smeared field; and (2) the pentacene monolayer screens the field from underneath.

The measured electric field gradient as a function of bias voltage shows a linear response as expected (Figure 2b). The slope of the linear response curve is greater when measured above pentacene islands because of the polarization contribution of the pentacene layer. Surface potential differences between the tip and sample can be obtained from Figure 2b by measuring the intercept of the linear response curve on the bias voltage axis. We obtain a tip surface potential of 0.05 V higher than that of SiO₂ but 0.45 V lower than that of pentacene. The surface electrostatic potential also defines the vacuum level in the electronic band structure of materials.²⁰ Therefore, the vacuum level on pentacene is 0.5 V lower than that on silicon dioxide. The interfacial dipole creates a misalignment between the vacuum levels of the two materials.

Is this large interfacial dipole consistent with other results? Interfacial dipoles are commonly observed at organic/metal interfaces;^{20–22} for example, photoemission spectroscopy shows dipoles between pentacene films and samarium²³ and between pentacene and Au(111).²⁴ On the other hand, some organic/organic interfaces show no interface dipole while others have dipole shifts of 0.1–0.5 eV. There is no general theoretical understanding of these data.²¹ Our 0.5 eV interfacial dipole between SiO₂ and pentacene contradicts the conclusion of a recent photoemission study of pentacene on an unannealed, 1-nm wet chemical oxide;²⁵ also, our pentacene sample was air-exposed unlike their study. We discuss this paper in the following section on thin oxides.

If the interface dipole is affected by environmental factors such as moisture and oxygen, or alternatively, if it is altered by device operation such as in bias–stress experiments, then a shift in TFT device gate bias would be required to reach the same net field in the pentacene channel. This represents a plausible explanation for observed rigid shifts in the transconductance characteristics.^{3,8}

Partial Fermi Level Pinning at the Pentacene SiO₂ Interface. Table 1 shows that the vacuum level of bare SiO₂ on an n-type Si substrate (Sb-doped, 0.008–0.03 Ω-cm) is about 0.46 V higher than that on a p-type Si (B-doped, 0.005–0.01 Ω-cm). Since the substrate is electrically wired to the scanning probe, this difference reflects the Fermi level difference between the two substrates when they are electrically isolated. The 0.46 eV surface Fermi level difference is significantly smaller than the 1.1 eV Si band gap. A reduced Fermi level swing at the interface compared to the bulk is frequently seen in Si/SiO₂²⁶ and attributed to band bending at the Si/SiO₂ interface. Previous UHV SKPM and C–V measurements show that Si dangling bond states at the interface causes a net space charge region

that is different in n-type and p-type Si and reduces the difference between them. The Fermi level is partially pinned.^{12,27}

Since the 2-nm oxide is thin enough for electrons and holes to tunnel across at the experimental time scale, an electric equilibrium is reached and the Fermi level is aligned across the 2-nm oxide layer. This contributes to the vacuum level shift above the pentacene in addition to the intrinsic interfacial dipole at the pentacene/SiO₂ interface (as on the thick oxide). In one extreme scenario, the pentacene/SiO₂ interface could be completely clean with no gap states, and the Fermi level is thus free to move with respect to the pentacene band structure at the interface. In this case, the Fermi level alignment requirement does not affect the vacuum level; therefore, the overall interface dipole and the vacuum level shift should be independent of whether the Si substrate was n-type or p-type, and the surface potential difference between the two substrates would remain 0.46 V. In the other extreme scenario, the Fermi level could be completely pinned at the interface because of high density of gap states. In this case, Fermi level alignment across the thin oxide would require an extra component of interfacial dipole that shifts the whole band structure of pentacene with respect to that of Si and SiO₂. The observed total vacuum level shift between the SiO₂ and pentacene will then depend on the doping of Si substrate, but the surface potential difference between the two substrates on pentacene islands would become zero because the Fermi level is pinned down.

The experimentally observed pentacene/SiO₂ interface behaves between these two limiting cases of no gap states and a high density of gap states. The Fermi level difference on pentacene islands between the n- and p-type substrate is 0.19 eV (Table 1). Compared to the 0.46 eV difference on bare SiO₂, the Fermi level difference is reduced on pentacene but not yet completely pinned. Of significance, however, is the observation that most of the reduction occurs for the p-type substrate. We suggest that electronic states, specifically hole traps at the SiO₂/pentacene interface (or in the pentacene islands), are populated by charge transfer across the oxide. Such population results in an extra interfacial dipole, which shifts the energy of all levels in the pentacene band structure until the Fermi level aligns with that of Si across the oxide. The n- and p- type Si substrates differ by 0.46 eV in the Fermi level; thus, the amount of extra interfacial dipole and the resulting overall vacuum level shift also differ on the two substrates. The observed 0.19 eV shift indicates the density of gap states is just enough for a partial Fermi level pinning at the interface.

C–V measurements show that the Si/SiO₂ P_b centers generate a symmetric interface state density within the gap;²⁷ therefore, we approximate the Fermi level at the Si/SiO₂ interface to be at $E_c - 0.3$ eV and $E_v + 0.3$ eV for n-type and p-type substrates, respectively. With the knowledge of the conduction band offset between the Si and SiO₂ of 3.2 eV,^{26,28} the electron affinity of SiO₂ of 0.95 eV,²⁹ and the electron affinity of pentacene of 2.9 eV,¹⁸ we estimate the Fermi level at the pentacene/SiO₂ interface to be $E_c - 1.6$ eV, or equivalently, $E_v + 0.6$ eV on n-type Si and $E_c - 1.9$ eV or $E_v + 0.3$ eV on p-type Si substrate. The observed Fermi level, which averaged between n- and p-type substrates, lies around 0.45 eV above E_v and is similar to that reported in recent experiments on pentacene single-crystal TFTs.³⁰

What causes these additional gap states associated with pentacene? Recent density functional calculations show that chemical impurities induced by hydrogen, oxygen, or moisture give rise to electrically active gap states in pentacene solid.³¹ In this connection, ambient exposure affects transport in organic

TFTs.³² We exposed the sample to 0.1 Pa of oxygen for a short time (<2 h) as a first attempt to examine the oxygen effect on the pentacene/SiO₂ interface. As shown in Figure 3 and Table 1, no significant change in surface potential difference between pentacene and SiO₂ was observed on either n- or p-type substrate. The vacuum levels relative to the probe tip (Table 1) become about 0.4 V lower than that in UHV, on both SiO₂ and pentacene. Considering that the sample was exposed to the ambient for about 10 min before the UHV measurement, the interface could be rather insensitive to further exposure to oxygen. The recent pentacene/SiO₂ photoemission study employed a 1-nm SiO₂ layer prepared using wet chemistry, without further annealing to remove the dangling bonds.²⁵ Considering the very thin oxide, the Fermi level of the pentacene/SiO₂ interface should align with that of the Si/SiO₂ in their sample. It seems likely that the high density of P_b centers pins the Fermi level around the center of the Si band gap in the sample and leads to an apparent vacuum level shift (at the pentacene/SiO₂) between what we observe in our n- and p-type substrates.

Conclusion

We find a pentacene/SiO₂ dipole of about 0.5 V on the thick oxide, whose origin is attributed largely to intrinsic contact potential differences between SiO₂ and pentacene. On the thin oxide, this dipole is modified by an additional interface dipole of opposite direction that is associated with charge transferred across the thin oxide, that is, Fermi level alignment. The observation of partial Fermi level pinning at 0.3–0.6 eV above the pentacene valence band indicates that there are gap states, predominantly hole traps associated with pentacene in this energy range. It will be important in the future to study how these states vary with exposure to ambient. Our study demonstrates the usefulness of EFM and SKPM in interface studies on insulating substrates.

Acknowledgment. The authors acknowledge D. V. Lang and R. Martel for constructive discussions and critical reading of the manuscript. We thank R. Martel and P. Avouris for use of SKPM apparatus under partial O₂ pressure and T. Graham for help in cleaning silicon wafers. This work has been primarily supported by the Nanoscale Science and Engineering Initiative of the National Science Foundation under NSF Award Number CHE-0117752 and by the New York State Office of Science, Technology, and Academic Research (NYSTAR).

References and Notes

- (1) Lin, Y. Y.; Gundlach, D. J.; Nelson, S. F.; Jackson, T. N. *IEEE Trans. Electron Devices* **1997**, *44*, 1325–1331.
- (2) Jackson, N.; Lin, Y. Y.; Gundlach, D. J.; Klauk, H. *IEEE J. Sel. Top. Quantum Electron.* **1998**, *4*, 100–104.
- (3) Dimitrakopoulos, C. D.; Malenfant, P. R. L. *Adv. Mater.* **2002**, *14*, 99–117.
- (4) Horowitz, G. *Adv. Mater.* **1998**, *10*, 365–377.
- (5) Karl, N.; Kraft, K. H.; Marktanner, J.; Munch, M.; Schatz, F.; Stehle, R.; Uhde, H. M. *J. Vac. Sci. Technol., A* **1999**, *17*, 2318–2328.
- (6) Nelson, S. F.; Lin, Y. Y.; Gundlach, D. J.; Jackson, T. N. *Appl. Phys. Lett.* **1998**, *72*, 1854–1856.
- (7) Warta, W.; Karl, N. *Phys. Rev. B* **1985**, *32*, 1172–1182.
- (8) Knipp, D.; Street, R. A.; Volkel, A.; Ho, J. *J. Appl. Phys.* **2003**, *93*, 347–355.
- (9) Volkel, A. R.; Street, R. A.; Knipp, D. *Phys. Rev. B* **2002**, *66*, art. no.195336.
- (10) Yang, Y. S.; Kim, S. H.; Lee, J. I.; Chu, H. Y.; Do, L. M.; Lee, H.; Oh, J.; Zyung, T.; Ryu, M. K.; Jang, M. S. *Appl. Phys. Lett.* **2002**, *80*, 1595–1597.
- (11) Ludeke, R.; Cartier, E. *Microelectron. Eng.* **2001**, *59*, 259–263.
- (12) Ludeke, R.; Cartier, E. *Appl. Phys. Lett.* **2001**, *78*, 3998–4000.
- (13) Kikukawa, A.; Hosaka, S.; Imura, R. *Appl. Phys. Lett.* **1995**, *66*, 3510–3512.

- (14) Burgi, L.; Sirringhaus, H.; Friend, R. H. *Appl. Phys. Lett.* **2002**, *80*, 2913–2915.
- (15) Cherniavskaya, O.; Chen, L. W.; Islam, M. A.; Brus, L. *Nano Lett.* **2003**, *3*, 497–501.
- (16) Cherniavskaya, O.; Chen, L. W.; Weng, V.; Yuditsky, L.; Brus, L. E. *J. Phys. Chem. B* **2003**, *107*, 1525–1531.
- (17) Weimer, A. W. *Carbide, Nitride and Boride materials: synthesis and processing*; Chapman & Hall: New York, 1997.
- (18) Pope, M.; Swenberg, C. E. *electronic Processes in Organic Crystals and Polymers*, 2nd ed.; Oxford University Press: New York, 1999.
- (19) Demkov, A. A.; Fonseca, L. R. C.; Tomfohr, J.; Sankey, O. F. *MRS Symp. Proc.* **2004**, *786*, 29.
- (20) Ishii, H.; Sugiyama, K.; Ito, E.; Seki, K. *Adv. Mater.* **1999**, *11*, 972–972.
- (21) Hill, I. G.; Milliron, D.; Schwartz, J.; Kahn, A. *Appl. Surf. Sci.* **2000**, *166*, 354–362.
- (22) Ishii, H.; Sugiyama, K.; Yoshimura, D.; Ito, E.; Ouchi, Y.; Seki, K. *IEEE J. Sel. Top. Quantum Electron.* **1998**, *4*, 24–33.
- (23) Koch, N.; Ghijsen, J.; Johnson, R. L.; Schwartz, J.; Pireaux, J. J.; Kahn, A. *J. Phys. Chem. B* **2002**, *106*, 4192–4196.
- (24) Schroeder, P. G.; France, C. B.; Park, J. B.; Parkinson, B. A. *J. Appl. Phys.* **2002**, *91*, 3010–3014.
- (25) Watkins, N. J.; Gao, Y. *J. Appl. Phys.* **2003**, *94*, 5782–5786.
- (26) Balk, P. In *The Si-SiO₂ system*; Balk, P., Ed.; Elsevier Science: Amsterdam, 1988; pp 1–20.
- (27) Chen, M. C.; Lang, D. V. *Phys. Rev. Lett.* **1983**, *51*, 427–429.
- (28) Keister, J. W.; Rowe, J. E.; Kolodziej, J. J.; Niimi, H.; Madey, T. E.; Lucovsky, G. *J. Vac. Sci. Technol., B* **1999**, *17*, 1831–1835.
- (29) Robertson, J. *J. Vac. Sci. Technol. B* **2000**, *18*, 1785–1791.
- (30) Butko, V. Y.; Chi, X.; Lang, D. V.; Ramirez, A. P. *Appl. Phys. Lett.* **2003**, *83*, 4773–4775.
- (31) Northrup, J. E.; Chabiny, M. L. *Phys. Rev. B* **2003**, *68*, 041202(R).
- (32) Zhu, Z. T.; Mason, J. T.; Dieckmann, R.; Malliaras, G. G. *Appl. Phys. Lett.* **2002**, *81*, 4643–4645.